journal

J. Am. Ceram. Soc., **96** [5] 1570–1576 (2013)
DOI: 10.1111/jace.12246

TEM Study of the High-Temperature Oxidation Behavior of Hot-Pressed ZrB_2–SiC Composites

Young-Hoon Seong, Seung Jun Lee, and Do Kyung Kim*,†

Department of Materials Science and Engineering, Korea Advanced Institute of Science and Technology (KAIST), Yuseong-gu, Daejeon 305-701, Republic of Korea

The oxidation behaviors of ZrB_2- 30 vol% SiC composites were investigated at 1500°C in air and under reducing conditions with oxygen partial pressures of 10^4 and 10^{-8} Pa, respectively. The oxidation of ZrB_2 and SiC were analyzed using transmission electron microscopy (TEM). Due to kinetic difference of oxidation behavior, the three layers (surface silica-rich layer, oxide layer, and unreacted layer) were observed over a wide area of specimen in air, while the two layers (oxide layer, and unreacted layer) were observed over a narrow area in specimen under reducing condition. In oxide layer, the ZrB_2 was oxidized to ZrO_2 accompanied by division into small grains and the shape was also changed from faceted to round. This layer also consisted of amorphous SiO_2 with residual SiC and found dispersed in TEM. Based on TEM analysis of ZrB_2–SiC composites tested under air and low oxygen partial pressure, the ZrB_2 begins to oxidize preferentially and the SiC remained without any changes at the interface between oxidized layer and unreacted layer.

I. Introduction

The transition-metal borides, carbides, and nitrides are classified as ultra-high-temperature ceramics (UHTCs). The UHTCs possess unique properties, including high melting points (>3200°C), good mechanical properties, strong oxidation resistance, and chemical inertness.[1–4] Because of this, the interest in UHTCs has increased in the field of aerospace applications, for applications such as a thermal protection systems (TPS) on hypersonic aerospace vehicles and reusable atmospheric reentry vehicles. Among the UHTCs, ZrB_2 has the lowest theoretical density (6.09 g/cm^3), and has good thermal shock resistance because of its high thermal conductivity (65–135 W/mK).[5] These attributes could be advantageous for TPS and other aerospace applications.[6–16] Many attempts have been made to enhance the oxidation resistance of ZrB_2-based materials through the use of appropriate additives. The most common additive is SiC, which enhances the oxidation resistance via the formation of SiO_2[1,16] as well as mechanical properties and sinterability.[17–20] The oxidation behaviors of ZrB_2–SiC composites have been well-defined previously.[21–24] When ZrB_2–SiC composite is exposed to oxidizing environments (at a temperature of 1500°C), it forms a layer structure consisting of the following (1) a continuous, silica-rich layer, (2) an SiC depletion layer, and (3) an unreacted layer. This surface silica-rich layer prohibits the transport of oxygen through the oxide scales, and allows the ZrB_2–SiC composite to show parabolic mass gain kinetics.[1,21]

Under reentry conditions, however, molecular oxygen will be dissociated, due to the impact with the leading edge of the wing and/or nose cap structure at hypersonic velocities.[25,26] Therefore, the O:O_2 ratio (i.e., the oxygen partial pressure) will be reduced during reentry. The oxidation mechanisms of SiC in the UHTCs are different at different oxygen partial pressures.[25] When the pO_2 is high (>10^{-5} Pa), SiC is oxidized and transformed to a viscous SiO_2 phase at 1500°C. On the other hand, when the pO_2 is low (<10^{-5} Pa), SiC is transformed to a SiO phase with high vapor pressure at 1500°C.[25,27] Thus, along with temperature, the oxygen partial pressure is an important parameter in evaluating the oxidation resistance of UHTCs. There are several methods to evaluate the high-temperature oxidation behaviors of UHTCs. Typically, high-temperature oxidation tests are conducted in a furnace, which is a useful tool for high-temperature oxidation behavior because of the accurate control over the atmosphere and temperature that it allows.

There are many reports of improved oxidation resistance, which have mainly been analyzed using SEM and energy dispersive X-ray spectroscopy (EDS). The analysis of the microstructural shape and phase changes in ZrB_2 and SiC after oxidation is also important and observation of the ZrB_2/ZrO_2 and SiC/SiO_2 interfaces after oxidation improves our understanding of the oxidation behavior at high temperature with varying pO_2. There are few reports which observe the microstructure of oxidized ZrB_2–SiC composites using transmission electron microscopy (TEM).[28] L. F. He studied that the kinetics of isothermal oxidation behavior of $Zr_2Al_3C_4$ at 500°C–1000°C and analyzed it using TEM.[29] In this article, we report an investigation of the oxidation of SiC and ZrB_2 and their oxidized phases after oxidation tests in air and at low oxygen partial pressure. In this research, we aim to provide basic understanding of oxidation mechanism of ZrB_2–SiC composite by TEM analysis.

II. Experimental Procedures

(1) Preparation

Commercially available raw powders were used in this study. ZrB_2 powder (Hexagonal, $a = b = 3.17$ Å, $c = 3.53$ Å, *P6/mmm*, size 3–5 μm, >99%, Grade A; H.C. Starck, Munich, Germany) and α-SiC powder (Hexagonal, 6H-polytype, $a = b = 3.07$ Å, $c = 15.08$ Å, *P63mc*, average size 0.45 μm, 98.5%, UF25; H.C. Starck) were used for hot-pressing. The batches consisted of 70 vol% of ZrB_2 powder and 30 vol% of SiC powder. Many previous studies have reported that ZrB_2- 30 vol% SiC composites showed improved sinterability and mechanical properties, and notably high-temperature oxidation resistance.[8,22,30–34] Therefore, composites with 70 vol% ZrB_2 and 30 vol% SiC were used for the oxidation tests in this study.

Before hot-pressing, to reduce the particle size, the ZrB_2 raw powders were vibration milled for 30 min, using steel balls (~3 mm diameter spheres) and steel container; The median particle size and particle size distribution of vibration-milled

W. Fahrenholtz—contributing editor

Manuscript No. 32016. Received September 8, 2012; approved February 1, 2013.
*Member, The American Ceramic Society.
†Author to whom correspondence should be addressed. e-mail: dkkim@kaist.ac.kr

ZrB_2 powder were D_{50} = 0.31 μm and D_{99}/D_{50} = 1.99, while D_{50} = 4.16 μm and D_{99}/D_{50} = 2.76 in as-received ZrB_2 powder, respectively. During the vibration milling, 3.1 wt% of Fe impurity was introduced to ZrB_2 powder due to wear of steel balls. Fe impurity was reduced to 0.042 wt% level by acid treatment (3 M HCl, 1 h). The ZrB_2 powder were subsequently mixed with 30 vol% SiC powder and milled for 24 h in polyethylene bottles, with pure ethanol as the solvent and ZrO_2 balls (~4 mm diameter spheres) as the milling media. The powders were then carefully dried in a rotating evaporator, to prevent phase separation between the ZrB_2 (ρ = 6.09 g/cm^3) and the SiC (ρ = 3.21 g/cm^3). After drying, the powders were crushed with a mortar and sieved using 325 mesh sieves.

The powders were densified using hot pressing (HP20-1000-3560; Thermal Technology Inc., CA), with a temperature of 1950°C and a pressure of 32 MPa applied for 2 h in a graphite furnace, under an argon atmosphere. The powders were loaded into an 18-mm diameter boron nitride coated graphite die. The furnace was heated to 1800°C at a rate of 20°C/min, and then heated to 1950°C at a rate of 10°C/min with uniaxial pressure of 32 MPa. Above 800°C, both a thermocouple and a pyrometer (Infrared Thermometer, 620 A; Konica Minolta, Tokyo, Japan) were used to monitor the temperature of the furnace and the graphite die. When the die temperature reached 1800°C, a uniaxial load of 32 MPa was applied. After 120 min, the furnace was cooled to room temperature at a rate of 10°C/min, and the load was removed when the die temperature dropped below 1500°C. Specimens with a diameter of ~18 mm and a thickness of ~6.5 mm were fabricated, and samples with dimensions of 4 mm × 4 mm × 3 mm were diced from the specimens for the oxidation tests. The samples prepared for the oxidation tests are listed in Table I.

(2) Oxidation

The oxidation tests were performed using a horizontal tube furnace equipped with a $MoSi_2$ heating element. Before the tests, specimens were prepared using conventional polishing with a diamond abrasive, down to a 1 μm finish. They were then placed on an alumina boat filled with ZrO_2 balls as a buffer layer, and inserted into the center of the furnace, where the thermocouple was located. The oxidation tests were conducted at 1500°C for 10 h, under an air (Z3S-H) and low oxygen partial pressure ($pO_2 = 10^{-8}$ Pa) atmosphere (Z3S-L). The heating and cooling rates were both 5°C/min. To create low pO_2 atmosphere conditions, CO gas containing 2000 ppm CO_2 was used, which produced an oxygen partial pressure of ~10^{-8} Pa at 1500°C. This oxygen partial pressure was selected based on the information obtained from a thermodynamic model, which predicted an oxygen partial pressure in the SiC-depleted region during the oxidation of the ZrB_2–SiC composite system.[25] The alumina (Al_2O_3, 99.9% purity, 60 mm outer diameter × 5 mm wall thickness × 1 m length) tube was used for CO/CO_2 gas flowing and ends of the tube were sealed using gastight end caps. A gas flow was maintained with a flow rate of ~100 cm^3/min.

Table I. Summary of ZrB_2–SiC Specimens: Compositions, Designations, Relative Density, and Conditions in the Oxidation Tests

Composition (volume ratio)		ZrB_2:SiC = 7:3	
Designations		Z3S-H	Z3S-L
Relative density (%)		99.5	99.8
Oxidation test conditions	Oxygen partial pressure (Pa)	2×10^4 Air, high pO_2	10^{-8} CO/CO_2, low pO_2
	Temperature (°C)	1500	
	Time (h)	10	

(3) Characterization

The densities of the hot-pressed specimens were measured using the Archimedes method, and the theoretical densities of the composites were calculated using the rule of mixture. The microstructures of the cross-sections of both the as-made and oxidized specimens were characterized using scanning electron microscopy (FE-SEM; Philips, XL30 FEG, Eindhoven, Netherlands). To analyze the microstructures of the vertical sections before and after the tests, the specimens for both cases were cross-sectioned and mounted in epoxy, carefully polished with a diamond abrasive down to a 1 μm finish, and cleaned in an ultrasonic bath with acetone. The thicknesses of the resulting reaction layers were measured from the polished cross-sections. The tested specimens were prepared for TEM observations using ion thinning performed using a focused ion beam system (FIB; Quanta 3-D FEG, FEI, Eindhoven, Netherlands). Bright field (BF) images, SAED patterns, high-resolution TEM (HRTEM) images, and EDS data were acquired using a transmission electron microscope (Tecnai G^2 F30 S-twin, FEI, Eindhoven, Netherland) operating at 300 kV. The thermo-gravimetric (TG) properties of the ZrB_2 and SiC starting powders were analyzed using a TG/DTA instrument (TGA 92-18; SETARAM, Caluire, France). The temperature was raised to 1400°C at a rate of 10°C/min.

III. Results and Discussion

(1) Characterization of Sintered Composite

The bulk densities for the hot-pressed billets were measured, yielding densities of 5.22 and 5.25 g/cm^3. The theoretical density of the ZrB_2- 30 vol% SiC composite was 5.23 g/cm^3, determined using a rule of mixture calculation (6.09 g/cm^3 for ZrB_2, and 3.21 g/cm^3 for SiC). Several assumptions for using a rule of mixture were used as follows: the 30 vol% SiC grains were well dispersed in 70 vol% ZrB_2 matrix and there are no reaction, substitution, and solid solution between ZrB_2 and SiC. The relative densities of specimens were over 99.5% to near theoretical density. This indicated that the porosity did not have a significant effect on the oxidation behavior.

Figure 1(a) shows a bright field TEM image of the hot-pressed ZrB_2–SiC composite. The black grains in the figure are ZrB_2, and the white grains are SiC. Intergranular faceted SiC grains with a grain size of 0.5–2.0 μm were observed at the ZrB_2 triple and quadruple junctions. The ZrB_2 grains also

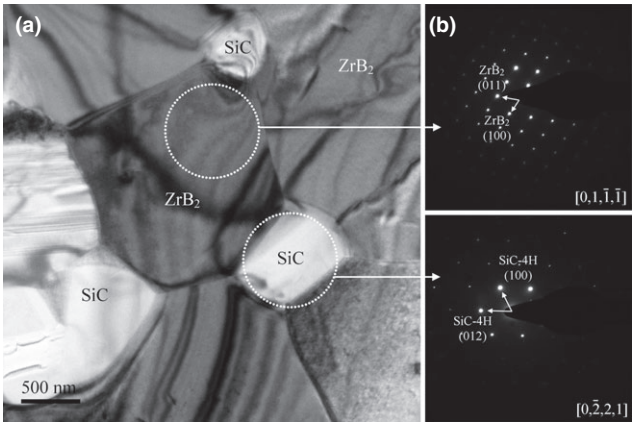

Fig. 1. Typical BF image of as-sintered ZrB_2- 30 vol% SiC composite. Intergranular SiC grains were located at the triple and quadruple junctions of the ZrB_2 grains. The inset SAED patterns taken from circled areas are showing [01$\bar{1}$1] zone axis pattern from ZrB_2 and [0$\bar{1}$21] zone axis pattern from SiC.

showed a faceted shape, with grain sizes of 3–6 μm. The inset SAED patterns taken from the circled areas are $[01\bar{1}\bar{1}]$ zone axis pattern of hexagonal ZrB_2 and $[0\bar{2}21]$ zone axis pattern of SiC-4H polytype (hexagonal structure) in Fig. 1(a). The SiC-6H starting powder might partially transform to 4H-type during sintering and the most stable polytypes of silicon carbide at 1800°C–2000°C were 4H and 6H.[35]

(2) Oxidation Tests

Figure 2 shows the reacted depth as a function of exposure time for the ZrB_2–SiC specimens oxidized in air and low pO_2 (10^{-8} Pa) atmosphere at 1500°C. In air, the shape of parabolic plots of oxidized depth versus time indicates that oxidation follows the parabolic rate law. The parabolic rate law of oxidation kinetics implies that the oxidation of ZrB_2–SiC composite in air is controlled by diffusion. It means the formed silica-rich oxide scale [reaction (1)] is protective because it is dense and smooth as seen in Fig. 3(a). Under low oxygen partial pressure (10^{-8} Pa), the oxidation kinetics at 1500°C is divided into two parts, parabolic kinetics at the starting 3 h and linear kinetics thereafter. In other words, oxidation kinetics deviates from the parabolic law and follow a linear law after 3 h of oxidation time. This indicates that the rate-limiting of oxide growth changes from the diffusion of oxygen through the reaction product layer [reactions (1) and (2)]; above 1300°C and 1100°C, respectively) to reaction between oxygen and SiC (reaction (3), SiO vaporizing below pO_2 ~8.8×10^{-13} Pa at 1500°C), and SiO dissociation from SiO_2 (reaction (4); range of $10^{-5} > pO_2 > 8.8 \times 10^{-13}$ Pa at 1500°C).[25,36] The parabolic-linear transition could be explained as the result of the gradual interconnection of the defects, such as pores crack and grain boundary.[29] The connectivity of oxidized ZrB_2–SiC grains becomes rough and loose and the number of grain-boundary interconnection is increased. Due to low oxygen partial pressure, the amount of SiO, which has relatively high partial pressure (~38.1 Pa) from SiO_2 increases greatly, possibly resulting in the formation of pores. When the defects interconnect with each other to form oxygen path (diffusion and transport) channels, the parabolic-linear transition of oxidation kinetics happens.

$$SiC(s) + 3/2O_2(g) \rightarrow SiO_2(l) + CO(g) \quad (1)$$

$$ZrB_3(s) + 5/2O_2(g) \rightarrow ZrO_2(s) + B_2O_3 \quad (2)$$

$$SiC(s) + O_2(g) \rightarrow SiO(g) + CO(g) \quad (3)$$

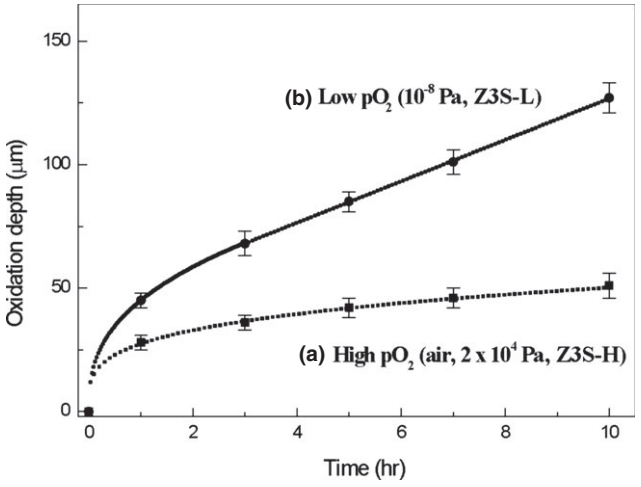

Fig. 2. Thickness of oxidation layer with time for exposure of ZrB_2- 30 vol% SiC at 1500°C (a) in air (2×10^4 Pa, Z3S-H) and (b) under low oxygen partial pressure (10^{-8} Pa, Z3S-L).

$$SiO_2(l) \rightarrow SiO(g) + 1/2O_2 \quad (4)$$

Figure 3 shows cross-sectional SEM images of the materials that were oxidized at 1500°C for 10 h in (a) air (2×10^4 Pa) and (b) under low oxygen partial pressure (10^{-8} Pa). The oxidation of the Z3S-H [Fig. 3(a)] composites at 1500°C produced structures consisting of four layers: a surface silica-rich layer, an oxide layer, a ZrO_2/ZrB_2–SiC layer, and an unreacted layer. The thickness of the oxidized layers (silica-rich layer + oxide layer) was 45 ± 5 μm. Several previous studies reported that three layers (SiO_2 layer (with $SiO_2 + ZrO_2$ layer: observed in some cases), SiC-depleted layer, unreacted layer) were consistently formed after oxidation tests at 1500°C.[1,16,21,23–25] Because the ZrB_2 and SiC phases oxidize rapidly, it results in the formation of a ZrO_2 layer and silica-rich layer, via reactions (2) and (1), respectively.[18]

However, three different layers (silica-rich layer, oxide layer ($SiO_2 + ZrO_2$), and unreacted layer) were observed in this study; there was no SiC-depleted layer and the oxide layer consisted of ZrO_2 and amorphous SiO_2 contained unreacted SiC. (Therefore, we call this layer "oxide layer" in this study) The formation of the SiC-depleted layer in the ZrB_2–SiC system depends not only on the surrounding pressure and temperature conditions but also on the volume distribution of the SiC in the ZrB_2 matrix.[32] In some cases, concretely, SiC-depleted layer is not formed because of the volume ratio of SiC/ZrB_2, SiC distribution, and internal oxygen partial pressure. The volume ratio of SiC and ZrB_2 is 3:7 in this study, and it is considered that the SiC fraction is relatively high. The high fraction of SiC increases the degree of SiC interconnectivity. The pO_2 value in this region cannot be defined clearly, but it is above 8.8×10^{-13} Pa (boundary condition of reaction (3) is dependent on the oxygen partial pressure), considering the pO_2 for the ZrB_2–ZrO_2 equilibrium at 1500°C.[36] Therefore, the SiC is oxidized to an amorphous SiO_2 phase rapidly and it disperses along the ZrO_2 grain boundaries at 1500°C. The reaction (1) was more dominant than reaction (3) in this region. Consequentially, the SiO_2 phase was increased by the internal

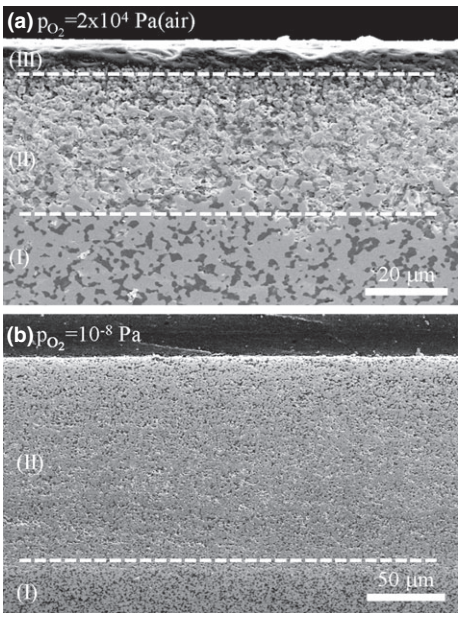

Fig. 3. Cross-sectional SEM micrographs of oxidized ZrB_2- 30 vol% SiC composite (1500°C, 10 h). (a) Z3S-H and (b) Z3S-L showing a layered structure comprising an unreacted ZrB_2–SiC layer (I), an oxide layer (II), and a uniform layer of SiO_2 (III, only in Z3S-H). The oxidized layer in Z3S-H was thinner than that observed in Z3S-L.

oxygen partial pressure and decreased amount of SiO (g) evaporation.

The SiO_2 oxide scale on the surface is protective in an air atmosphere, because SiO_2 is significantly less volatile than B_2O_3, and acts as a barrier against inward oxygen transport.[1,21,25] The volume increase upon the oxidation of ZrB_2–SiC could also have been one of the driving forces for the amorphous SiO_2 viscous flow to the surface.[37] Thus, a silica-rich layer provides the passive oxidation behavior with a parabolic increase in oxidation depth. The oxide layer was located underneath the surface SiO_2 layer, and the microstructure of this region was similar to the original structure, because the SiC was removed by active or passive oxidation.[38] The SiO_2 might have remained at the ZrO_2 grain boundaries under certain conditions (conditions for passive oxidation of SiC, temperature range from 1200°C to 1600°C and above $pO_2 > 8.8 \times 10^{-13}$ Pa).[25,32] At the interface between the unreacted layer and the oxide layer, even under high oxygen partial pressure conditions ($pO_2 > 10^{-5}$ Pa), SiO (g) phase was transported to the surface via reaction (3), after reaction (1) occurred near the interface between the unreacted layer and the oxide layer. This occurred because this region had a lower oxygen partial pressure compared with that outside of the specimen. However, it consequently showed passive oxidation behavior because of the surface SiO_2 oxide scale that acted as a SiO (g) barrier layer.

In contrast to Z3S-H, in Z3S-L, the silica-rich layer was not formed on the surface and, only two layers (oxide layer, unreacted layer) were observed. The depth of the oxidized layers [layer II of Fig. 3(b)] was 135 ± 3 μm, much thicker than that measured for Z3S-H. A few studies have reported on the oxidation behaviors of the ZrB_2–SiC system under reducing conditions. Rezaie *et al*. explained that the high vapor pressure of SiO (g) under reducing conditions leads to the active oxidation of SiC.[25] The SiC is removed directly by active oxidation (10^{-15} Pa $< pO_2 < 8.8 \times 10^{-13}$ Pa) [reaction (3)], or it oxidizes to SiO_2 [reaction (1)], which is then removed by volatilization (8.8×10^{-13} Pa $< pO_2 < 10^{-5}$ Pa) [reaction (4)]. Likewise, the ZrB_2 is stable below $pO_2 \sim 1.9 \times 10^{-11}$ Pa, or will oxidize to form ZrO_2 and B_2O_3. In other words, the oxidation behaviors of the ZrB_2-SiC system depend on the precise pO_2. The oxygen diffuses to the inside of the bulk more easily, due to the absence of a SiO_2 layer on the surface and the smaller amounts of SiO_2 at the grain boundaries under reducing conditions.

(A) Oxidation Test at High-pO_2 Atmosphere (Air, 2×10^4 Pa): Figure 4(a) shows a typical BF image taken from the region slightly below the interface between the unreacted layer (I) and the oxide layer (II) in Fig. 3(a). Several samples were prepared to find this interface at varying depths. In this region, some ZrB_2 grains were oxidized and their shapes were changed from faceted to uneven, while the SiC grains remained stable. Some parts of the ZrB_2 grain began to oxidize, and its phase was transformed. The ZrB_2 grain was, therefore, divided into two grains: unreacted ZrB_2 grain and oxidized ZrB_2 (ZrO_2 phase). It is well-known that below 1100°C, the oxidation of SiC (cr) is much slower than that of ZrB_2,[39] and that above 1100°C, SiC is oxidized rapidly via reaction (1) to form SiO_2. At 1500°C, the oxidation of the ZrB_2 phase exhibited rapid linear kinetics. Even when the oxygen partial pressure of this region was much lower than that of the surface, the ZrB_2 phase was oxidized preferentially, while the SiC phase was rarely oxidized. Figure 4(b) shows an HRTEM image taken from the squared area in Fig. 4(a), at the interface between partially oxidized ZrB_2 and unreacted ZrB_2. The atomic arrangement of the left region clearly revealed it to be a hexagonal structure with a planar spacing of 3.5487 Å for the {001} plane of the ZrB_2 phase. The atomic arrangement of the right region also clearly showed structure and planar spacing. A monoclinic ZrO_2 structure was revealed and the planar spacing of the right region did not match any of the SiC polytypes. This

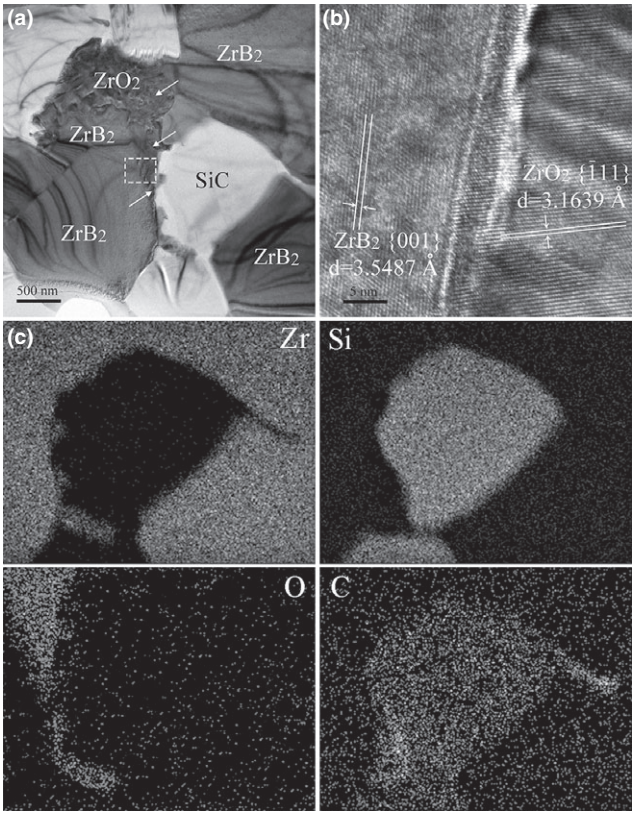

Fig. 4. (a) BF image of the top part in the unreacted ZrB_2–SiC layer. Immediately below the oxidized layer of Z3S-H, the ZrB_2 grain and grain boundary begin to transform into a ZrO_2 phase. (b) HRTEM image of the ZrB_2/ZrO_2 interface taken from the squared area in (a). (c) The elements maps of partially oxidized ZrB_2 grain and SiC grain.

region had a planar spacing of 3.1639 Å for the $\{\bar{1}11\}$ plane of the monoclinic ZrO_2 phase. There is a large difference in lattice volume at the interface between the ZrO_2 ($V_{lattice} = 140.7$ Å^3 in monoclinic ZrO_2,) and ZrB_2 ($V_{lattice} = 30.7$ Å^3) grains. Therefore, stress might be concentrated at the interface between ZrO_2 phase and ZrB_2 phase. The deformation (transformation) also occurred to minimize the strain energy at this incoherent interface. The interface between ZrO_2 and ZrB_2 might have moved leftward (in the direction of the inward ZrB_2 grain) as the oxidation time increased. The partially oxidized ZrB_2 grain was also confirmed by element maps in Fig. 4(c). The Zr and O elements were detected at right region which had a planar spacing of the monoclinic ZrO_2 phase in ZrB_2 grain and grain boundary while Si and C elements were only detected in SiC grain. From the results of Fig. 4, it seems the oxygen might be diffused and oxidized along the ZrB_2 grain boundary preferentially and preceded to inward ZrB_2 grain.

The BF image of Fig. 5 shows the microstructure of the oxide interlayer [layer II of Fig. 3(a)] between the surface SiO_2 layer and the unreacted Z3S-H layer. It is closer to the outer silica-rich layer than to the un-oxidized ZrB_2–SiC layer. The microstructure was different from that of the unreacted layer, and the shape of the grains changed from faceted to round. Almost all of the ZrB_2 grains were oxidized to form an oxide phase (ZrO_2); the grains were then divided into smaller grains with a size of 0.5–1.5 μm, and they changed shape to minimize the surface energy. Many grain boundaries were created and the number of oxygen diffusion path was increased due to the oxidation of ZrB_2. In addition, the number of oxygen vacancies in the non-stoichiometric zirconium oxides ($ZrO_{2-\delta}$) might increase due to the low oxygen partial pressure.[40] They accelerated the oxidation of the specimen, until the surface was covered with the SiO_2 amorphous

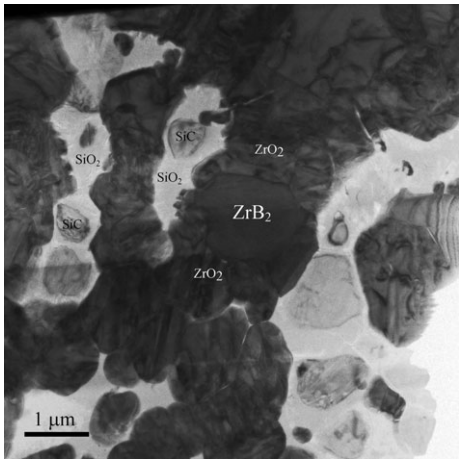

Fig. 5. BF image of the interlayer between the surface SiO_2 glass layer and the unreacted layer. The oxide phases (ZrO_2 and amorphous SiO_2) were mostly observed, and the unreacted ZrB_2 and SiC grains remained in this layer.

phase. The surface of SiC grain also oxidized and transformed to amorphous phase of SiO_2 with volumetric increase and viscous flow. Unreacted SiC remained at the midmost of SiO_2 and showed island structure.

The SiC grains might also have been oxidized and transformed to give an amorphous SiO_2 phase with flowing viscously into the grain boundaries. Based on the volatility diagram,[25,38,41] the pO_2 in this region was not low enough to allow the active oxidizing reaction [reaction (3)]. The pO_2 for this region was above 8.8×10^{-13} Pa, considering the pO_2 for the ZrB_2–ZrO_2 equilibrium at 1500°C. If the pO_2 value was lower than 8.8×10^{-13} Pa, the SiC in the ZrB_2–SiC would oxidize to form SiO (g), and a layer of SiO_2 (l) would not form in this region. A slight pO_2 gradient was likely to exist across the layers.

(B) Oxidation Test at Low-pO_2 Atmosphere (10^{-8} Pa): Figure 6 shows an STEM image of the specimen tested at low oxygen partial pressure; the image was taken from the interface between the unreacted layer (II) and the oxidized layer [layer I of Fig. 3(b)], which was thinned using FIB before TEM analysis. Although the analyzed area was much narrower than that of Z3S-H, two small layers (ZrO_2/ZrB_2–SiC section and ZrO_2/ZrB_2+SiC/SiO_2 section) were clearly observed in one specimen (except the unreacted ZrB_2–SiC section), while similar two sections were seen over a wide area in case of Z3S-H (Figs. 4 and 5). Because the oxidation behavior of ZrB_2-SiC at 1500°C under low pO_2 is kinetically much active. Section 1 of Fig. 6 shows the unreacted region with faceted ZrB_2, and SiC grains. In section 2, some ZrB_2 grains are oxidized and their shapes are changed, but the SiC grains are stable. Section 3 contains ZrB_2 and SiC grains with ZrO_2 grains and SiO_2 amorphous phase.

Figure 7(a) shows a high-magnification BF image taken from section 2 (the interlayer between the unreacted layer and the oxide layer) in Fig. 6. ZrB_2, ZrO_2, and SiC grains were observed. Some ZrB_2 grains were oxidized and their shapes were changed, and some ZrB_2 grains were divided into several small ZrO_2 grains after the oxidation; the SiC was stable in this region. Figure 7(b) shows an HRTEM image taken from the circled area in Fig. 7(a). The interface between the fully oxidized ZrO_2 grain and the unreacted ZrB_2 grain was observed. The atomic arrangement of the grain on the left side of circled area clearly revealed a monoclinic structure with a planar spacing of 3.71 Å for the {011} plane of the ZrO_2 phase. The atomic arrangement of the grain on the right side of circled area also clearly showed planar spacing and its structure. A hexagonal structure and a ZrB_2 phase were revealed. This grain had a planar spacing of 3.58 Å for the {001} plane of the ZrB_2 phase.

Figure 8 shows a high-magnification BF image taken from section 3 of Fig. 6. The amorphous SiO_2 phase was dispersed along the grain boundaries between the ZrO_2 grains and the unreacted SiC grains, or at the SiC/SiC grain boundaries. The SiO_2 phase flowed viscously, and wetted the SiC and

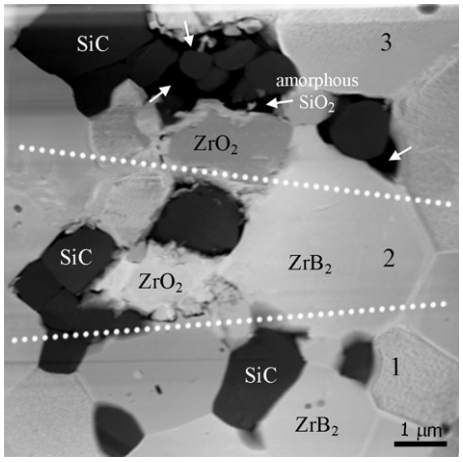

Fig. 6. STEM image of the interface between the unreacted boride layer (Fig. 3(b)-I) and the oxidized layer (Fig. 3 (b)-II) in Z3S-L. All of the sections (1: unreacted section, 2: ZrO_2/ZrB_2–SiC section, and 3: ZrO_2/ZrB_2 + SiC/SiO_2 section) existed in one specimen of Z3S-L.

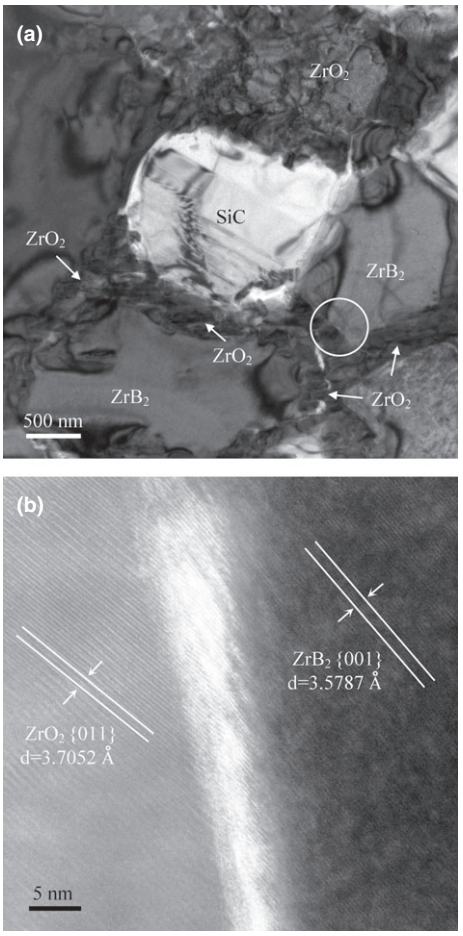

Fig. 7. (a) TEM BF image of the ZrO_2–SiC layer. (Section 2 of Fig. 5) The ZrB_2 grains and grain boundaries began to oxidize and transform into ZrO_2, while the SiC grain maintained its phase. (b) HRTEM image and d-spacing values for the ZrB_2/ZrO_2 interface from the circled area in (a).

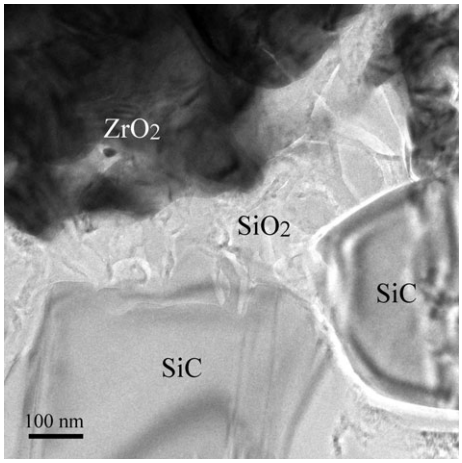

Fig. 8. TEM BF image of the reacted oxide layer. (Section 3 of Fig. 5) The ZrO_2 and SiC grains were observed and amorphous SiO_2 was dispersed at grain boundary.

ZrO_2 grains after the SiC grains were oxidized and transformed to amorphous phase.

In both cases (air and reducing conditions), the oxidation started from the formation of ZrO_2 at the interface between oxidized layer and unreacted layer. When ZrB_2 is oxidized, grain boundaries of ZrB_2 started to transform to ZrO_2 phase first. Then the oxidation proceeded through grain boundaries with oxygen diffusion and finally the oxidation extened to inward ZrB_2 grains. This phenomenon can be seen from images in Figs. 5 and 7, the ZrB_2 grain is located inside and ZrO_2 is located outside of ZrB_2 grain boundary. After that, the grains were divided into several small ZrO_2 grains and the shape changed from faceted to round. As mentioned above, the oxygen might transport through ZrB_2 grain boundaries, ZrO_2 grain boundaries (created by rounded ZrO_2 grains formation) and oxygen vacancies in the non-stoichiometric $ZrO_{2-\delta}$. Due to the multipath for diffusion of oxygen, the oxidation kinetics of ZrB_2 was controlled by diffusion of oxygen through ZrB_2 grain boundaries. The oxidation rate of SiC was relatively slower than that of ZrB_2. The oxidation behavior of SiC started from the surface of SiC grain with transformation to amorphous SiO_2 phase and the oxidation proceeded to inside the grain. When the SiO_2 formed and covered on the surface of SiC grain, the oxygen is difficult to react with SiC because surface SiO_2 phase act as a barrier for oxygen diffusion. The surface SiO_2 prohibited the oxygen diffusion inside and retarded the oxidation of SiC. Therefore, unreacted SiC remained on the surface, SiO_2 at the grain boundaries, and the oxidation kinetics of SiC was controlled by diffusion of oxygen at surface SiO_2, i.e., diffusion-controlled kinetics.

Figure 9(a) shows a TEM BF image of the oxide region in the oxidized layer [layer II of Fig. 3(b)] of Z3S-L. The amorphous SiO_2 phase was observed to disperse along the ZrO_2 grain boundaries, including many pores. Figure 9(b) shows a magnified BF image of a grain boundary composed of amorphous phase SiO_2 and a pore in Fig. 9(a). The microstructure of this region was similar to that of the oxidized layer at the interface between the unreacted layer and the oxidized layer, as shown in Fig. 8 (section 3 of Fig. 6). However, many pores were observed in dispersed SiO_2 at the grain boundaries with absence of SiC phase after the test—despite the fact that the region was sufficiently oxidized—indicated that the oxygen partial pressure of this region was not low enough to rapidly evaporate the SiO phase from the SiO_2 phase (pSiO was low at this pO_2). Based on the thermodynamic calculations and the volatility diagram, the range of oxygen partial pressure that allowed active oxidation in the volatile SiO (g) phase is from 10^{-15} Pa to 10^{-5} Pa.[42] The SiO phase evaporated directly from the SiC phase in the

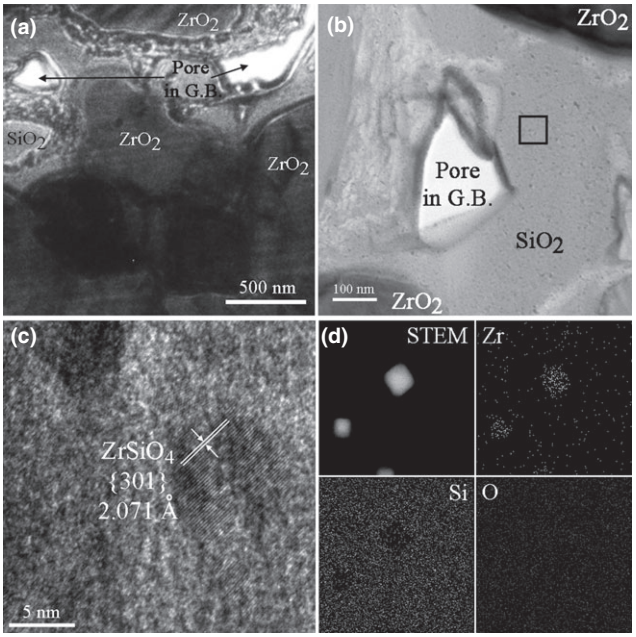

Fig. 9. (a) TEM BF image of the reacted oxide layer (II) in Z3SL; the amorphous SiO_2 dispersed along the ZrO_2 grain boundaries with pores. (b) The magnified image of (a). The nano-sized particles were observed (black spots) in amorphous SiO_2. (c) The highly magnified image of particles in (b). These particles have been identified as $ZrSiO_4$ by atomic arrangement with a planar spacing of 2.071 Å for the {301} plane of the $ZrSiO_4$ phase and (d) Zr, Si, O element maps.

range of oxygen partial pressure from 10^{-15} Pa to 8.8×10^{-13} Pa reaction (3), whereas the SiC transformed to a SiO_2 amorphous phase reaction (1) and then, the SiO phase evaporated from the SiO_2 phase with a relatively low partial vapor pressure after oxidation in the range of oxygen partial pressure from 8.8×10^{-13} Pa to 10^{-5} Pa reaction (4).[25] The amorphous SiO_2 phase therefore remained at the grain boundaries with pores, because the oxygen partial pressure for Z3S-L was 10^{-8} Pa in this study. The pores in the amorphous SiO_2 phase originated from the evaporation of the SiO (g) phase, and using $pO_2 = 10^{-8}$ Pa, reaction (4) can be used to calculate pSiO = 38.15 Pa. This showed that the oxidation kinetics of the ZrB_2–SiC composite under low partial pressure of oxygen at 1500°C is different from those of the composite in ambient pressures, and the existence of protective layer on the surface has an important role to the oxidation kinetics of ZrB_2–SiC composites. Figure 9(c) shows a highly magnified BF image of amorphous SiO_2 at the grain boundary taken from the squared area in Fig. 9(b). There were many particles in amorphous SiO_2 with size of ~5 nm. Also, the atomic arrangement was observed with a planar spacing of 2.071 Å for the {301} plane of the $ZrSiO_4$ phase. It is confirmed by element maps in Fig. 9(d) and the Zr, Si, and O were detected as particles. This result was caused by further reaction between ZrO_2 and amorphous SiO_2. The interstitial silicon diffuses and dissolves into crystalline ZrO_2 until the solution limit is reached when ZrO_2 and amorphous silica coexisted, thereafter by precipitation of $ZrSiO_4$.[43]

IV. Conclusions

The ZrB_2-30 vol% SiC composites were oxidized in air ($pO_2 = 10^4$ Pa), and under reducing conditions ($pO_2 = 10^{-8}$ Pa) at 1500°C for 10 h. The microstructures and oxidation depths of the specimens were observed using SEM and phase transformation and microstructure of the grains/grain boundaries on each layer were analyzed using TEM.

Based on TEM results, the three layers (surface SiO_2 layer, oxide layer, and unreacted layers) were observed in Z3S-H and the two layers (oxide layer, and unreacted layer) were observed in Z3S-L with varying depths after oxidation test. The SiO_2 and residual SiC were dispersed in whole oxide layer in Z3S-H, because of the structural distribution of SiC in the ZrB_2 matrix and internal oxygen partial pressure. In contrast, active oxidation behavior and no surface SiO_2 layer were observed in Z3S-L, and the amorphous SiO_2 phase also remained at the ZrO_2 grain boundaries in Z3S-L.

The results from the TEM analysis, in both cases (air and reducing conditions), ZrB_2 was oxidized and transformed to ZrO_2 phase firstly and then, SiC was oxidized at the interface between unreacted layer and oxidized layer. The oxidation and transformation of ZrB_2 was started from grain boundaries and the oxidation proceeded to the inside of grain which showed outside ZrO_2 and inside ZrB_2 structure. Then, the grains were divided into several ZrO_2 grains after fully oxidizing with the shape changing from facet to round. The SiC started to oxidize and transform into SiO_2 from the surface of SiC grain. After that, the SiO_2 was dispersed in grain boundaries in whole oxide layer of composite due to high viscosity and volumetric increase. The unreacted SiC existed in amorphous SiO_2 which has an island structure.

The oxidation kinetics of ZrB_2 might be controlled by O_2 diffusion and transport through the ZrB_2 grain boundaries and ZrO_2 grain boundaries, respectively, and the oxidation kinetics of SiC might be controlled by O_2 diffusion through SiO_2 because surface SiO_2 acted as an oxygen diffusion barrier. The oxidation behavior in structural changes was similar, but the oxidation kinetics was different. TEM analysis is one of the good approaches for understanding oxidation behaviors of ZrB_2–SiC-based UHTCs.

Acknowledgments

This work was supported by Defense Acquisition Program Administration and Agency for Defense Development under the contract UD110093CD and the Priority Research Centers Program through the NRF funded by MEST (2009-0094041).

References

[1]W. G. Fahrenholtz, G. E. Hilmas, I. G. Talmy, and J. A. Zaykoski, "Refractory Diborides of Zirconium and Hafnium," *J. Am. Ceram. Soc.*, **90** [5] 1347–64 (2007).

[2]N. P. Bansal, "Ultra High Temperature Ceramic Composites"; pp. 197–224 in *Handbook of Ceramic Composites*, Edited by N. P. Bansal. Springer, NY, 2004.

[3]M. M. Opeka, I. G. Talmy, and J. A. Zaykoski, "Oxidation-Based Materials Selection for 2000°C+ Hypersonic Aerosurfaces: Theoretical Considerations and Historical Experience," *J. Mater. Sci.*, **39** [19] 5887–904 (2004).

[4]S. J. Lee, E. S. Kang, S. S. Baek, and D. K. Kim, "Reactive Hot Pressing and Oxidation Behavior of Hf-Based Ultra-High-Temperature Ceramics," *Surf. Rev. Lett.*, **17** [2] 215–21 (2010).

[5]R. A. Cutler, "Engineering Properties of Borides"; pp. 787–803 in *Ceramics and Glasses, Engineered Materials Handbook*, Vol. 4, Edited by S. J. Schneider Jr. ASM International, Materials Park, OH, 1991.

[6]S. R. Levine, E. J. Opila, M. C. Halbig, J. D. Kiser, M. Singh, and J. A. Salem, "Evaluation of Ultra-High Temperature Ceramics for Aeropropulsion Use," *J. Eur. Ceram. Soc.*, **22** [14–15] 2757–67 (2002).

[7]D. M. Van Wie, D. G. Drewry, D. E. King, and C. M. Hudson, "The Hypersonic Environment: Required Operating Conditions and Design Challenges," *J. Mater. Sci.*, **39** [19] 5915–24 (2004).

[8]A. L. Chamberlain, W. G. Fahrenholtz, and G. E. Hilmas, "Oxidation of ZrB_2-SiC Ceramics Under Atmosphere and Reentry Conditions," *Refract. Appl. Trans*, **1** [2] 1–8 (2005).

[9]F. Monteverde and L. Scatteia, "Resistance to Thermal Shock and to Oxidation of Metal Diborides-SiC Ceramics for Aerospace Application," *J. Am. Ceram. Soc.*, **90** [4] 1130–8 (2007).

[10]F. Monteverde and A. Bellosi, "Oxidation of ZrB_2-Based Ceramics in Dry Air," *J. Electrochem. Soc.*, **150** [11] B552–9 (2003).

[11]F. Monteverde, A. Bellosi, and L. Scatteia, "Processing and Properties of Ultra-High Temperature Ceramics for Space Applications," *Mater. Sci. Eng., A*, **485** [1–2] 415–21 (2008).

[12]M. Gasch, D. Ellerby, E. Irby, S. Beckman, M. Gusman, and S. Johnson, "Processing, Properties and Arc Jet Oxidation of Hafnium Diboride/Silicon Carbide Ultra High Temperature Ceramics," *J. Mater. Sci.*, **39** [19] 5925–37 (2004).

[13]G. J. Zhang, Z. Y. Deng, N. Kondo, J. F. Yang, and T. Ohji, "Reactive Hot Pressing of ZrB_2-SiC Composites," *J. Am. Ceram. Soc.*, **83** [9] 2330–2 (2000).

[14]A. L. Chamberlain, W. G. Fahrenholtz, G. E. Hilmas, and D. T. Ellerby, "High-Strength Zirconium Diboride-Based Ceramics," *J. Am. Ceram. Soc.*, **87** [6] 1170–2 (2004).

[15]W. W. Wu, G. J. Zhang, Y. M. Kan, and P. L. Wang, "Reactive Hot Pressing of ZrB_2-SiC-ZrC Composites at 1600 °C," *J. Am. Ceram. Soc.*, **91** [8] 2501–8 (2008).

[16]S. S. Hwang, A. L. Vasiliev, and N. P. Padture, "Improved Processing, and Oxidation-Resistance of ZrB_2 Ultra-High Temperature Ceramics Containing SiC Nanodispersoids," *Mater. Sci. Eng., A*, **464** [1–2] 216–24 (2007).

[17]M. M. Opeka, I. G. Talmy, E. J. Wuchina, J. A. Zaykoski, and S. J. Causey, "Mechanical, Thermal, and Oxidation Properties of Refractory Hafnium and Zirconium Compounds," *J. Eur. Ceram. Soc.*, **19** [13–14] 2405–14 (1999).

[18]W. C. Tripp, H. H. Davis, and H. C. Graham, "Effect of an SiC Addition on Oxidation of ZrB_2," *Am. Ceram. Soc. Bull.*, **52** [8] 612–6 (1973).

[19]X. C. Zhong and H. L. Zhao, "High-Temperature Properties of Refractory Composites," *Am. Ceram. Soc. Bull.*, **78** [7] 98–101 (1999).

[20]G. A. Pankov, G. A. Fomina, D. A. Ivanov, and G. E. Val'yano, "Strength and Scaling Resistance of a Composite Based on Zirconium Diboride," *Refractories*, **35** [9] 298–300 (1994).

[21]A. Rezaie, W. G. Fahrenholtz, and G. E. Hilmas, "Evolution of Structure During the Oxidation of Zirconium Diboride-Silicon Carbide in Air Up to 1500 °C," *J. Eur. Ceram. Soc.*, **27** [6] 2495–501 (2007).

[22]J. C. H. P. Hu, X. H. Zhang, and S. H. Meng, "Oxidation Behavior of Zirconium Diboride-Silicon Carbide at 1800 °C," *Scripta Mater.*, **57** [9] 825–8 (2007).

[23]S. J. Lee and D. K. Kim, "The Oxidation Behavior of ZrB_2-Based Mixed Boride," *Key Eng. Mater.*, **403**, 253–5 (2007).

[24]S. N. Karlsdottir, J. W. Halloran, and A. N. Grundy, "Zirconia Transport by Liquid Convection During Oxidation of Zirconium Diboride-Silicon Carbide," *J. Am. Ceram. Soc.*, **91** [1] 272–7 (2008).

[25]A. Rezaie, W. G. Fahrenholtz, and G. E. Hilmas, "Oxidation of Zirconium Diboride-Silicon Carbide at 1500 °C at a Low Partial Pressure of Oxygen," *J. Am. Ceram. Soc.*, **89** [10] 3240–5 (2006).

[26]A. Bongiorno, C. J. Forst, R. K. Kalia, J. Li, J. Marschall, A. Nakano, M. M. Opeka, I. G. Talmy, P. Vashishta, and S. Yip, "A Perspective on Modeling Materials in Extreme Environments: Oxidation of Ultrahigh-Temperature Ceramics," *MRS Bull.*, **31** [5] 410–8 (2006).

[27]N. S. Jacobson, "Corrosion of Silicon-Based Ceramics in Combustion Environments," *J. Am. Ceram. Soc.*, **76** [1] 3–28 (1993).

[28]D. D. Jayaseelan, E. Zapata-Solvas, P. Brown, and W. E. Lee, "*In Situ* Formation of Oxidation Resistant Refractory Coatings on SiC-Reinforced ZrB_2 Ultra High Temperature Ceramics," *J. Am. Ceram. Soc.*, **95** [4] 1247–54 (2012).

[29]L. F. He, Z. J. Lin, Y. W. Bao, M. S. Li, J. Y. Wang, and Y. C. Zhou, "Isothermal Oxidation of Bulk $Zr_2Al_3C_4$ at 500 to 1000 °C in Air," *J. Mater. Res.*, **23** [2] 359–66 (2008).

[30]S. N. Karlsdottir and J. W. Halloran, "Oxidation of ZrB_2-SiC: Influence of SiC Content on Solid and Liquid Oxide Phase Formation," *J. Am. Ceram. Soc.*, **92** [2] 481–6 (2009).

[31]P. Sarin, P. E. Driemeyer, R. P. Haggerty, D. K. Kim, J. L. Bell, Z. D. Apostolov, and W. M. Kriven, "*In Situ* Studies of Oxidation of ZrB_2 and ZrB_2-SiC Composites at High Temperatures," *J. Eur. Ceram. Soc.*, **30** [11] 2375–86 (2010).

[32]X. H. Zhang, P. Hu, and J. C. Han, "Structure Evolution of ZrB_2-SiC During the Oxidation in Air," *J. Mater. Res.*, **23** [7] 1961–72 (2008).

[33]C. A. Wang, H. Wang, Y. Huang, and D. Fang, "Preparation and Flame Ablation/Oxidation Behavior of ZrB_2/SiC Ultra-High Temperature Ceramic Composites," *Key Eng. Mater.*, **351**, 142–6 (2007).

[34]W. M. Guo and G. J. Zhang, "Oxidation Resistance and Strength Retention of ZrB_2-SiC Ceramics," *J. Eur. Ceram. Soc.*, **30** [11] 2387–95 (2010).

[35]N. W. Jepps and T. F. Page, "Polytypic Transformation in Silicon Carbide," *Progress in Crystal Growth and Characterization*, **7** [1–4] 259–307 (1983).

[36]W. G. Fahrenholtz, "Thermodynamic Analysis of ZrB_2-SiC Oxidation: Formation of a SiC-Depleted Region," *J. Am. Ceram. Soc.*, **90** [1] 143–8 (2007).

[37]S. N. Karlsdottir and J. W. Halloran, "Formation of Oxide Scales on Zirconium Diboride-Silicon Carbide Composites During Oxidation: Relation of Subscale Recession to Liquid Oxide Flow," *J. Am. Ceram. Soc.*, **91** [11] 3652–8 (2008).

[38]D. D. Jayaseelan, Y. Wang, G. E. Hilmas, W. G. Fahrenholtz, P. Brown, and W. E. Lee, "TEM Investigation of Hot Pressed-10 vol.% SiC-ZrB_2 Composite," *Adv. Appl. Ceram.*, **110** [1] 1–7 (2011).

[39]W. C. Tripp and H. C. Graham, "Thermogravimetric Study of Oxidation of ZrB_2 in Temperature Range of 800 °C to 1500 °C," *J. Electrochem. Soc.*, **118** [7] 1195–9 (1971).

[40]E. Opila, S. Levine, and J. Lorincz, "Oxidation of ZrB_2- and HfB_2- Based Ultra-High Temperature Ceramics: Effect of Ta Additions," *J. Mater. Sci.*, **39** [19] 5969–77 (2004).

[41]W. G. Fahrenholtz, "The ZrB_2 Volatility Diagram," *J. Am. Ceram. Soc.*, **88** [12] 3509–12 (2005).

[42]M. W. Chase Jr, *NIST-JANAF Thermochemical Tables*, 4th edn. American Institute of Physics, Woodbury, NY, 1998.

[43]S. Q. Guo, T. Mizuguchi, M. Ikegami, and Y. Kagawa, "Oxidation Behavior of ZrB_2-$MoSi_2$-SiC Composites in Air at 1500°C," *Ceramic International*, **37** [2] 585–91 (2011). □